The Luzon Strait experiment

Matthieu J. Mercier, Thomas Peacock, Sasan Saidi, Samuel Viboud, Henri Didelle, Louis Gostiaux, Joël Sommeria, Thierry Dauxois, Karl Helfrich

The Luzon Strait experiment

Matthieu Mercier[1], Thomas Peacock[1], Sasan Saidi[1], Samuel Viboud[2], Henri Didelle[2], Louis Gostiaux[2], Joel Sommeria[2], Thierry Dauxois[3] and Karl Helfrich[4]

[1] Department of Mechanical Engineering, Massachusetts Institute of Technology.
[2] Laboratoire des Écoulements Géophysiques et Industriels (LEGI), CNRS.
[3] Université de Lyon, Laboratoire de Physique, École Normale Supérieure de Lyon, CNRS.
[4] Woods Hole Oceanographic Institution.
mmercier@mit.edu

Abstract

We present preliminary results from a realistic experiment that took place at the Coriolis turntable (Grenoble, France) investigating the baroclinic tide generated at the Luzon Strait. Careful scalings of the spatial and temporal coordinates have been done to preserve dynamic similarity with the ocean's problem. The study of the barotropic and baroclinic diurnal tides reveals good agreement with observations and models.

1 Introduction

Internal tides are generated by the barotropic tides forcing the stratified medium over the bottom topography. In the ocean, roughly 1TW of energy is input into the internal tides from the semi-diurnal (M2) and diurnal (K1) barotropic tides (Garrett and Kunze (2007)). This energy radiates away and participates in mixing events that are important to the general circulation of the ocean, although several aspects (nature, location, efficiency) of these processes are still investigated.

Numerous studies have focused on idealized geometries, tackling the problem from several aspects. The internal tide generation from the Hawaiian ridge have been studied thanks to field studies (Pinkel and Rudnick (2006)) and numerical investigations (Johnston et al. (2003)). The more general problem of internal tide generation by an isolated sea mount have been the subject of many research works (Johnston et al. (2003); Pétrélis et al. (2006); Peacock et al. (2008); King et al. (2009); Echeverri et al. (2009)).

The Luzon Strait, located between Taiwan and the Philippines and connecting the Pacific Ocean to the South China Sea (SCS), is a good example of internal tide generation by complex bathymetry. Field studies (Ramp et al. (2004); Alford et al. (2010)) and satellite observations (Hsu and Liu (2000)) report strong internal tides propagating away from this double-ridge system, leading to some of the largest internal solitary waves observed worldwide. Large scale numerical simulations have also focused on the Luzon ridge system (Zhang et al. (2011)) but there currently exists no supporting laboratory experimental data.

The goal of these experiments is to bring insight into phenomena that are very difficult to observe during field studies and of high computational cost for numerical simulations, while generating a benchmark data set.

In the next section, we present the experimental setup before investigating in section 3 the geometry of the diurnal tide. We conclude in section 4.

2 Experimental setup

We have performed an unprecedented internal tide experiment at the Coriolis turntable, the world largest rotating table (13 m in diameter, 1 m deep) located in Grenoble (France). In this experiment, we model the generation of internal tides at the Luzon Strait using realistic topography and background stratification.

As can be seen in Fig. 1 (a), the topography is localized almost in the center of the tank, with vertical walls extending the North and South islands (Taiwan and the the Philippines respectively) as far as the sides of the tank, dividing it into two basins. The Pacific basin corresponds to the right-hand (West) side and the South China Sea (SCS) to the left-hand (East) side. Along the wall of the tank, some damping material (Blocksom matting added to a coarser grid) have been put to prevent reflection of the generated internal waves.

Barotropic tidal forcing is realized using two vertically-oscillating prismatic plungers pushing the full water column, and giving the opportunity to study harmonic forcing or mixed tides (ω_1 and ω_2 in Fig. 1 (a)). The amplitude of oscillation of each plunger can be changed from 1 to 5 cm. Two vertical walls are put in front of the plungers to block internal waves that could have been generated by the sharp edges of the prisms.

The region of interest considered for the topography is limited to the geographical region in between 120E and 123E in longitude and 18N and 23N in latitude, as can be seen in Fig. 1 (b). Furthermore, we restrict ourselves to the upper 3000 m of the ocean on both sides, since the turning points for the diurnal and semi diurnal tides for the stratification in this region are above this depth.

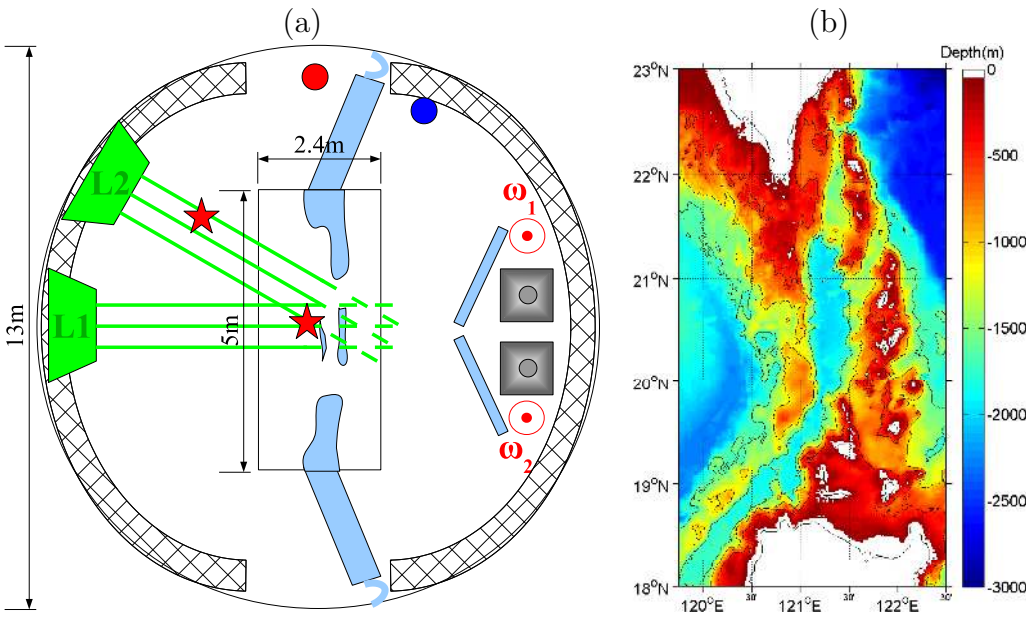

Figure 1: (a) Schematic of the experimental setup. (b) Contour map of the region of interest considered for the design of the topography (Smith & Sandwell, 1' resolution).

Finally, two types of stratification were considered, a weak and a strong one corresponding to typical conditions associated to winter and summer conditions. An example of the summer stratification is shown in Fig. 2 (a).

2.1 Instrumentation

Different techniques have been used to better understand the wavefield radiated from the ridge.

Elevations of the free surface have been obtained using ultrasonic transducers located approximatively 5 cm below the surface, a set of three in both the Pacific and the SCS basins (blue and red circles in Fig. 1 (a)). By measuring the time of an impulse to travel back and forth from the transducer to the free surface, we can monitor the signature of the barotropic tide at the free surface. The technique is very sensitive and allows measurements of elevation as small as ~ 0.05 mm.

Conductivity and temperature sensors (CT-probes) are used to measure isopycnal displacements in the vicinity of the pycnocline (red stars in Fig. 1 (a)). These probes mounted on a traverse can also measure the density profile.

Large horizontal views of the velocity field in a plane have been obtained using submerged white lights and specific particle seeding. We refer to this technique as "white" PIV which is based on the following approach. Taking advantage of the density profile considered (Fig. 2 (a)), buoyant particles with densities in a specific range, $[1.020, 1.023]$ g cm^{-3} in the case presented here, are used to create a thin sheet of particles all over the water tank. Images are recorded with several cameras looking through the free surface, more than 5 m above it, allowing for very large fields of view. More specifically, by computing the vertical profiles of the horizontal velocity of the first modes associated to the density profile (Fig. 2 (b)), we carefully choose the density range for the particles in order to catch the dynamics of the main modes, avoiding the depth of nodes of the vertical profiles where the motion of the particles is almost null. Finally, "classic" Particle Image Velocimetry

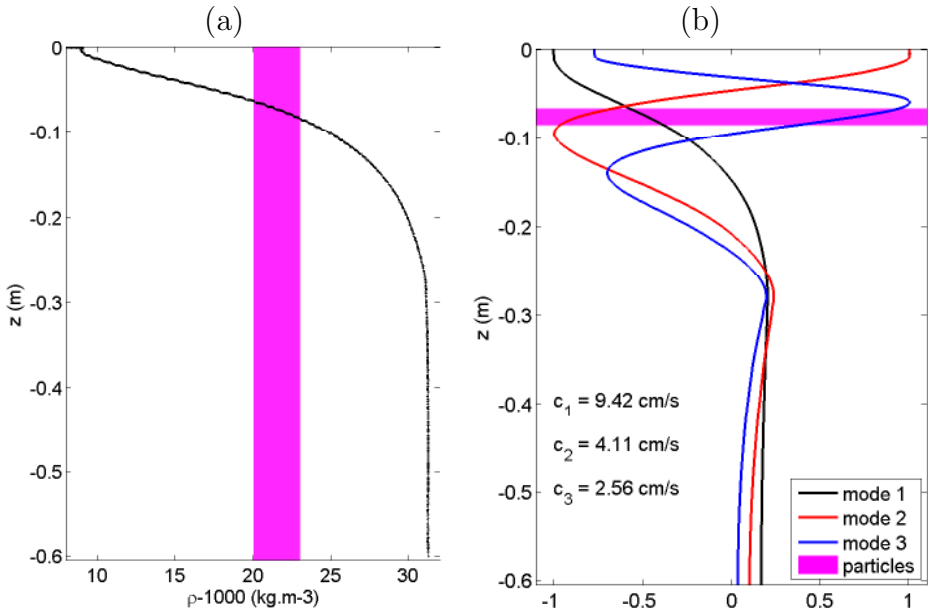

Figure 2: (a) An example of a laboratory density profile corresponding to a strong stratification. (b) Normalized vertical profiles of the horizontal velocity for the first three modes associated to the diurnal frequency, along with their speed of propagation c_i. The magenta boxes correspond to the density range for the buoyant particles used.

	U	ω	Q	N_{max}	H	L
units	m/s	rad/s	m^3/s	rad/s	km	km
Luzon	0.2	$0.7\ 10^{-4}$	$0.7\ 10^{8}$	$2\ 10^{-2}$	3	200
Lab	10^{-2}	0.2	$4\ 10^{-3}$	1.5	$6\ 10^{-4}$	$2\ 10^{-3}$

Table 1: Relevant values for the topography, stratification and barotropic tide from the Luzon Strait and the laboratory.

(PIV) in vertical planes is used to observe the radiated internal tide. Two series of vertical views have been considered (L1 and L2 in Fig. 1 (a)), based on the geometry of the radiated tide preliminary observed with horizontal views.

2.2 Dynamical similarity

Before the experiments, particular care was taken to achieve dynamical similarity with the oceanic problem. Parameters such as criticality, Froude number and excursion of the tides were all matched with those at the Luzon Strait. Different horizontal and vertical scalings, of $1/100000^e$ and $1/5000^e$ respectively, were chosen to accommodate the Coriolis turntable, leading to a change of slope by a factor 20. This effect was considered when scaling the stratification and forcing frequency, in order to keep criticality.

Typical values for the diurnal tide considered for the Luzon Strait as a large double-ridge system (*Luzon*) along with the ones obtained in the laboratory are provided in table 1. Some dimensionless parameters relevant to different internal tide generation mechanisms can thus be estimated. In both the Luzon Strait and the laboratory, the excursion of the tide $A = \frac{U}{\omega L}$ is of order 0.1, the horizontal Froude number $Fr_L = \frac{U}{NL}$ and the vertical one $Fr_H = \frac{U}{NH}$ are of order 10^{-3} and 10^{-2} respectively, and the criticality $\epsilon = \frac{H}{L \tan\theta}$ comparing the slope of the topography $\frac{H}{L}$ and the one of the internal waves $\tan\theta$ has values close to 1 although there are some specific locations on the topography associated to this value. The Reynolds number $Re = \frac{UL}{\nu}$ however cannot be reproduce at the laboratory scale, its value is roughly 10^8 in the ocean whereas only 10^3 in our experiments.

Although not presented here, experiments with background rotation have also been realized. Since it is not possible to scale independently the stratification N, the forcing frequency ω and the Coriolis frequency f while keeping criticality unchanged, we have decided to keep the ratio ω/f similar to the one in the Luzon Strait (1.4 for the diurnal tide).

3 Investigation of the diurnal tide

We have oriented our laboratory reference frame with respect to the geographic coordinates, to compare to realistic data. According to the spatial scaling considered, 1 kilometer corresponds to 1 centimeter and we have considered here 1 degree of longitude/latitude as 111 cm.

Such visualizations provide qualitative indications about the correct modeling of the bathymetry of the Luzon Strait. However, quantitative comparisons are under development based on two different approaches: one involving a three-dimensional scanner and the other based on extracting contours of the topography visualized during filling.

We focus here on the harmonic diurnal tide, which corresponds in our case to a forcing frequency $\omega = 0.206$ rad s^{-1}, with an amplitude of oscillation of the plunger $A_0 = 2$ cm.

3.1 Barotropic forcing

In order to study the barotropic forcing generated by the plunger, a series of experiments have been realized with homogeneous water of depth 60.4 cm. Measurements of the velocity in several horizontal planes using classic PIV have been used, thanks to a laser sheet located in the SCS basin. A drawback of this approach is the shadow regions induced by the complex topography.

A comparison of the geometry of the barotropic currents in the vicinity of the ridge is shown in Fig. 3, with data from the TOPEX/POSEIDON model (Egbert and Erofeeva (2002)) refered to as TPXO 7.1, and from horizontal PIV in a plane 5 cm below the surface. Although the resolution of the TPXO model does not equal the one obtained in

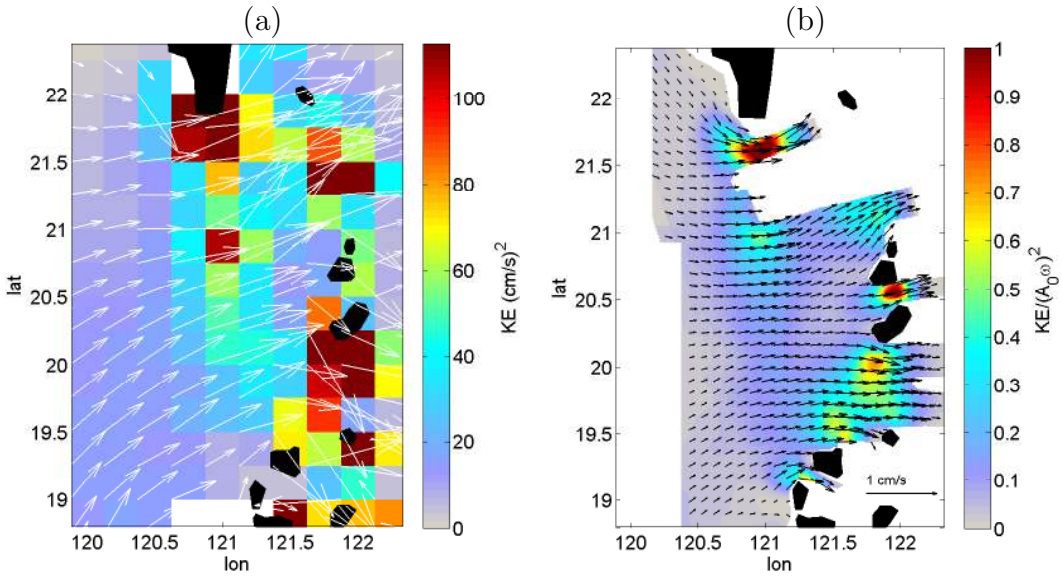

Figure 3: Kinetic energy map of the barotropic tide from (a) TPXO 7.1 model, and from (b) the experiments with a diurnal-like forcing ($\omega = 0.190$ rad s^{-1}).

the laboratory, both the intensity of the kinetic energy and the directions of the velocity (vectors) have very similar features.

Furthermore, one can observed in figure 3 (b) that the maximum velocities reached in the topography are of the same order than the velocity generated by the plunger ($\sim A_0\omega$). This remains true for other frequencies close to 0.2 rad s^{-1}, and for amplitudes smaller than 4 cm.

3.2 Baroclinic tide

Having verified the coherence of the barotropic tide generated, we can investigate the baroclinic tide generated in the case of a strong stratification (shown in Fig. 2 (a)).

The complete recording of the elevation of the free surface in each basin is shown in Fig. 4 (a), giving an indication of the steady-state reached rapidly for the barotropic tide

(after 5 periods). We have estimated the steady state for the baroclinic tide to be reached after approximatively 10 periods of forcing, with negligible amount of waves reflecting at the sides of the tank. This estimation is coherent with the time needed for the slowest low modes (mode 3 for instance) to propagate across the full SCS basin, higher modes being damped quickly.

The amplitude and phase of the eastward component of the velocity field, filtered at the forcing frequency over 8 periods (as indicated in Fig. 4 (a)) are shown in Fig. 4 (b) and (c).

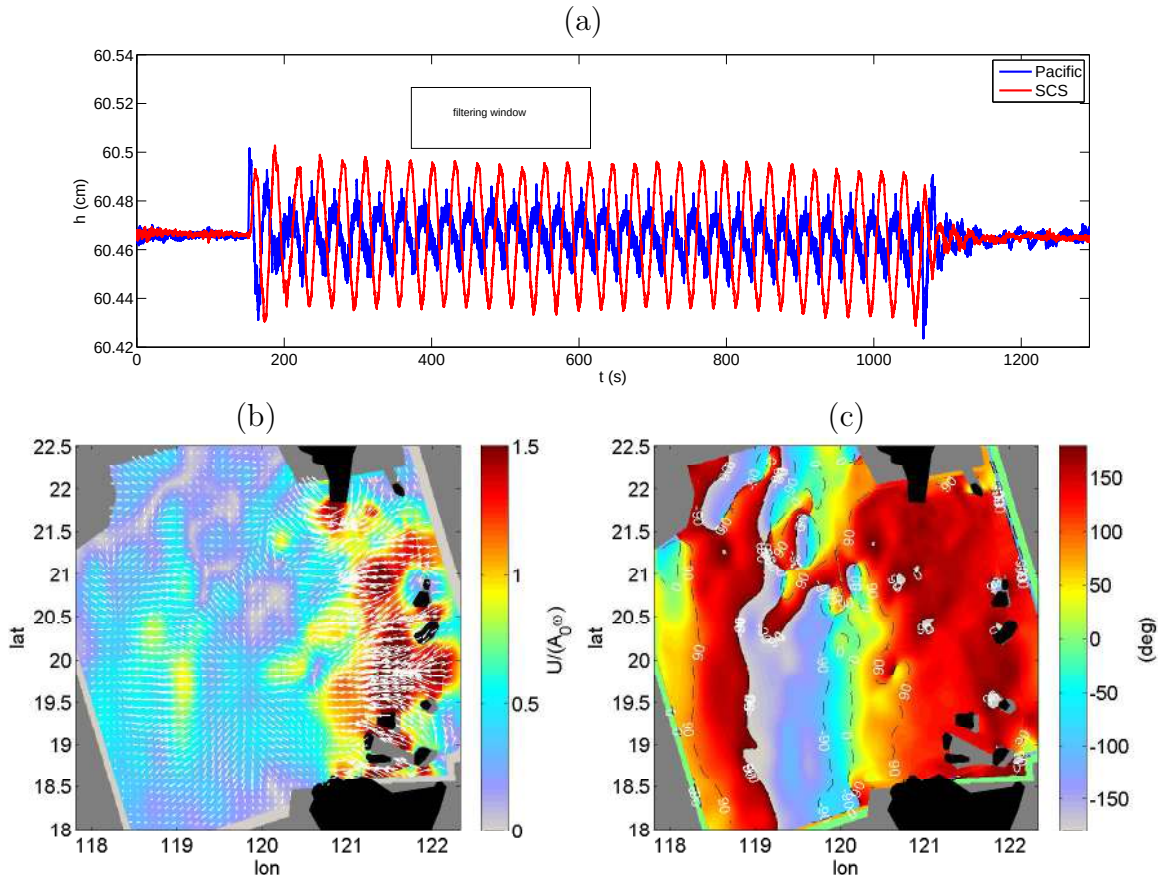

Figure 4: (a) Complete recording of the ultrasonic probes showing the elevation of the free surface in each basin, along with an indication of the time window used for the filtered data in (b) and (c). Map of the (b) amplitude and (c) phase of the eastward component of the velocity field filtered at $\omega = 0.206$ rad s^{-1}. Data have been collected using particle seeding in white PIV described in § 2.1, the gray regions indicate absence of data whereas the black regions correspond to islands.

First of all, the map of the phase of the velocity in Fig. 4 (c) gives a very clear indication of the direction of propagation of the radiated baroclinic tide. Lines of constant phase being in the North-South direction, the baroclinic tide propagates almost purely eastward. Estimation of the wavelength of the tide is difficult due to non-homogeneous gradient of the phase in this direction, indicating the presence of several modes radiating away from the strait. However, the dominant wavelength is of the order of 2.2 m, leading to horizontal phase velocity of 7.3 cm s^{-1}, close to the mode 1 estimate in Fig. 2 (b). It must be noticed that the phase is almost constant in the double-ridge system, which can be interpreted as a standing wave in between the two ridges.

The amplitude map, along with the velocity vectors, in Fig. 4 (b) reveals a strong activity in the double-ridge system as a whole, with eastward velocity up to 1.5 larger than the forcing. Some modulation of the amplitude in the SCS basin is also clearly visible with a spatial periodicity of the same order than the main wavelength estimated from the phase map. This modulation is actually due to the superposition of both the baroclinic and the barotropic tide in the observed velocity field. Hence, the wavelength of the barotropic tide being very large compared to the size of the tank, its superposition with the baroclinic wavefield leads to this spatial modulation.

Finally, results from numerical simulations by Jan et al. (2008) seem to be in agreement for the case of the diurnal tide, although the authors only show the baroclinic component.

4 Conclusion

A comprehensive study of the barotropic tide and baroclinic tide in the case of a realistic experiment modeling the Luzon Strait have been presented, with specific care taken to have a dynamic similarity with the oceanic problem. We have focused on the specific case of the diurnal tide with a strong stratification and small amplitude tide. However many more experiments associated to stronger forcing, semi-diurnal tide and mixed tides are still being analyzed.

The first results suggest that the baroclinic diurnal tide generated by the complex topography remains quasi-bidimensional in the far field, with a well defined direction of propagation (eastward), waves in the double-ridge system being in phase when filtered at the frequency of the barotropic tide.

More information concerning the modal content of the radiated baroclinic tide will be gained from the analysis of the vertical views and from the CT-probes recording. Finally, experiments with background rotation are the most expected to mimic observations made in the ocean.

References

Alford, M. H., Lien, R.-C., Simmons, H., Klymak, J., Ramp, S., Yang, Y. J., Tang, D., and Chang, M.-H. (2010). Speed and evolution of nonlinear internal waves transiting the South China Sea. *Journal of Physical Oceanography*, 40:1338–1355.

Echeverri, P., Flynn, M. R., Peacock, T., and Winters, K. B. (2009). Low-mode internal tide generation by topography: An experimental and numerical investigation. *Journal of Fluid Mechanics*, 638:91–108.

Egbert, G. D. and Erofeeva, S. Y. (2002). Efficient inverse modeling of barotropic ocean tides. *Journal of Atmospheric and Oceanic Technology*, 19:183–204.

Garrett, C. and Kunze, E. (2007). Internal tide generation in the deep ocean. *Annual Review of Fluid Mechanics*, 39:57–87.

Hsu, M.-K. and Liu, A. K. (2000). Nonlinear internal waves in the South China Sea. *Canadian Journal of Remote Sensing*, 26:72–81.

Jan, S., Lien, R.-C., and Ting, C.-H. (2008). Numerical study of baroclinic tides in luzon strait. *Journal of Oceanography*, 64:789–802.

Johnston, T. M. S., Merrifield, M. A., and Holloway, P. (2003). Internal tide scattering at the line islands ridge. *Journal of Geophysical Research*, 108 (C11):3365.

King, B., Zhang, H. P., and Swinney, H. L. (2009). Tidal flow over three-dimensional topography in a stratified fluid. *Physics of Fluids*, 21:116601.

Peacock, T., Echeverri, P., and Balmforth, N. J. (2008). An experimental investigation of internal wave beam generation by two-dimensional topography. *Journal of Physical Oceanography*, 38:235–242.

Pétrélis, F., Llewellyn Smith, S., and Young, W. R. (2006). Tidal conversion at a submarine ridge. *Journal of Physical Oceanography*, 36:1053–1071.

Pinkel, R. and Rudnick, D. (2006). Hawaii ocean mixing experiment (home), editorial. *Journal of Physical Oceanography*, 36:965–966.

Ramp, S. R., Tang, T. Y., Duda, T. F., Lynch, J. F., Liu, A. K., Chiu, C.-S., Bahr, F. L., Kim, H.-R., and Yang, Y.-J. (2004). Internal solitons in the northeastern South China Sea part i: Sources and deep water propagation. *IEEE Journal of Oceanic Engineering*, 29:1157–1181.

Zhang, Z., Fringer, O. B., and Ramp, S. R. (2011). Three-dimensional, nonhydrostatic numerical simulation of nonlinear internal wave generation and propagation in the south china sea. *Journal of Geophysical Research*, 116:C05022.